Small-Number Effects: A Third Stable State in a Genetic Bistable Toggle Switch

Rui Ma,[1] Jichao Wang,[2] Zhonghuai Hou,[1,*] and Haiyan Liu[2,†]

[1]School of Chemistry and Materials Science, University of Science and Technology of China, Hefei 230026, Anhui, China
[2]School of Life Sciences, University of Science and Technology of China, Hefei 230027, Anhui, China

(Received 18 July 2012; published 13 December 2012)

A genetic toggle switch was studied experimentally and theoretically. We have found an additional kinetic stable state where all the genes express very lowly, which is predicted to be unstable by dynamical systems theory. It can also stably coexist with the other two known stable states, although this coexistence is forbidden in a deterministic dynamical system. We analyze that this nontrivial phenomenon results from the discrete and fluctuate nature in such a small system, by comparing experimental results with modeling results of exact stochastic simulations and differential equations.

DOI: 10.1103/PhysRevLett.109.248107 PACS numbers: 87.18.−h, 05.40.Ca, 82.39.Rt, 87.10.−e

A living cell is a typical small system, where there are many biochemical processes forming reaction networks. To study the kinetics of them, reaction processes are often described by rate equations, which are a group of ordinary differential equations (ODEs). In such networks, the genetic toggle switch is a bistable biological element which has been investigated in cell differentiation, biocircuits, cellular memory, epigenetics, and development, etc. [1,2]. There is a kind of toggle switch based only on mutual inhibition [3,4], whose reaction kinetic characteristics might simply be described by a pair of ODEs. These equations predict at most two stable steady states (SSSs) and one unstable steady state (USS), as shown by the intersections of curves in Fig. 1(top layer). It is well known that stochastic fluctuation is not negligible in such a small system, so ODEs with noise terms should be used in simulation, forming a set of stochastic differential equations (SDEs). Exact stochastic simulation via kinetic Monte Carlo (KMC) algorithm is another choice.

Comparing with deterministic dynamical systems theory, the usual result of stochastic simulation does not significantly change the kinetic characteristics of a biochemical reaction network, and the fluctuation usually acts as a perturbation in it [5,6]. Specific to any kind of genetic toggle switch, previous experiments and simulations have proven that its characteristics accord with what the ODEs predict [3,7,8], even if an underlying mechanism modifies the ODE model [9]. Nevertheless, there are a few simulational works having captured some new kinetic stability via KMC simulations [10,11], including multistability [12]. However, the region around the traditional USS, where all the genes are silent (rarely expressing), is still unreachable. Furthermore, the underlying mechanism of how exact stochastic simulation gives rise to new kinetic stability remains to be elucidated.

In this Letter, we have experimentally and theoretically revealed an additional kinetic stable state nearby the traditionally regarded USS. The whole system could be from monostable to tristable under different conditions. Experimental results are illustrated in the middle layer of Fig. 1: all the regions where the real system converges are stable in the practical sense, even around theoretical USS. Exact stochastic simulation (bottom layer, their statistical results) and fluctuation analysis have been done to reveal the source of this additional kinetic stability: the discrete and fluctuate nature of molecule numbers, especially when they are often very close to or equal to zero. This class of small-number effects cannot be treated by the continuous differential-equation model, even if SDE was used—SDE simulations were performed by chemical Langevin equations (CLEs) with Gaussian noise terms, and their results are drawn as point density plots in the top layer of Fig. 1.

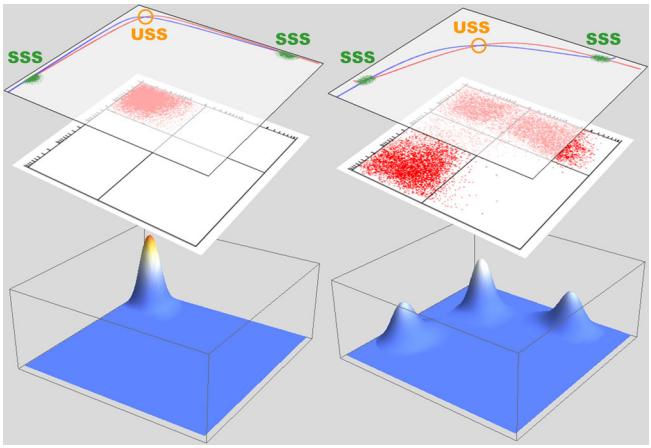

FIG. 1 (color online). Brief illustration of our main results. (Top layer) the predictions of stability analyses based on dynamical systems theory—systems should tend to converge toward SSS, as shown around SSS points by simulation results of Langevin equations, while keeping away from USS, but the realities are contrary to this prediction. (Middle layer) the fluorescence detection results in biochemical experiments; this real system has an additional stable state nearby the USS. (Bottom layer) the probability density functions of exact stochastic simulations' results; they are consistent with experimental results.

These density plots only surround the deterministic SSS points.

Thus, these are not simplex fluctuation phenomena, but composite effects presented in small reaction systems that have pivotal molecules fluctuating on the verge of extinction. It might have general significance of the systems with the same features, in reaction kinetics, population dynamics, and so on. Moreover, we have demonstrated that small-number effects can be taken advantage of to achieve special functions in small systems, which a macroscopic system cannot achieve conveniently.

The experimental details of our synthetic biological network (illustrated in Fig. 2) are listed in the Supplemental Material [13]. Based on this practical network, we got transition processes and a corresponding high-dimensional ODE model (Table S1 and S2 in the Supplemental Material [13]). By using steady-state approximation in a standard way, we can reduce that ODE model into a two-dimensional dynamical system, which facilitates for stability analysis, as follows:

$$\frac{d[A]}{dt} = \frac{\alpha_a}{1 + r_a[B]^n} - [A], \tag{1a}$$

$$\frac{d[B]}{dt} = \frac{\alpha_b}{1 + r_b[A]^m} - [B]. \tag{1b}$$

Refer to previous literature [3,14]; here, $\alpha_a(\alpha_b)$ denotes the expression efficiency for gene of $A(B)$; m and n are cooperativity coefficients; repressing strength coefficients r_a and r_b are extracted explicitly because we'd change them in our experiments [15]. For simplicity, a symmetric model is considered, i.e., $\alpha_a = \alpha_b$, $r_a = r_b = R$, $m = n = 2$, while the effects to be presented here will persist by dropping this condition. These equations describe the same steady-state kinetic characteristics as what high-dimensional model does. Their nullclines are drawn in Fig. 1 (top layer). Although the shape of nullclines changes with different repressing strength R, there are always three steady states: the intermediate one is unstable and the other two are stable.

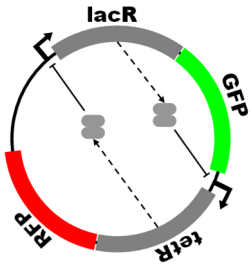

FIG. 2 (color online). Schematic illustration of the genetic toggle switch plasmid. Each promoter is repressed by a dimer of corresponding repressors. GFP and RFP are fluorescent proteins coexpressed with respective repressors, which act as reporters for presenting the current state of this toggle switch.

Specific to our experimental system (Fig. 2), repressor A (LacR) coexpresses with fluorescent reporter GFP; repressor B (TetR) coexpresses with RFP. (The reporters are attached by small stable RNA A (ssrA) fast degradation tags. For minimizing the competing for fast degradation pathway [16], we did not attach such tags onto the repressors.) One SSS corresponds to the state where LacR and GFP have high expression while TetR and RFP are suppressed, and vice versa for the other SSS. The only USS corresponds to the state where all kinds of proteins have little expression. In our experiments, we use fluorescence microscopy and fluorescence activated cell sorting (FACS) technology, which can detect only whether GFP/RFP is in existence, rather than repressors. Thus, according to the kinetic stability analysis, SSSs should be the green- or red-fluorescence state observed abundantly in this practical system; while the USS is a low- or no-fluorescence state which should not be presented in large amounts.

Surprisingly, when there is no inducer, the no-fluorescence state is the only one observed in our experiments, in all the feasible cell density or time that bacteria could be cultured [Fig. 3(b)]. More interestingly, when we add very low concentrations of two inducers together

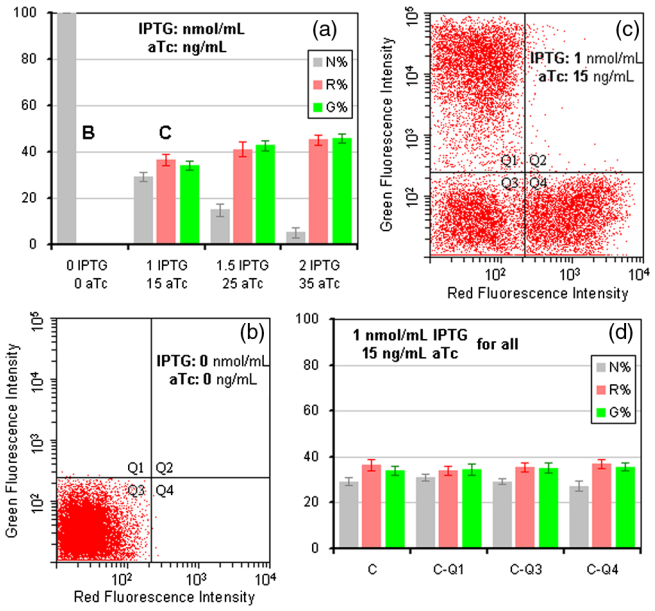

FIG. 3 (color online). Key results of FACS experiments. (a) Four groups of differentiation ratios under different conditions. The final concentrations of inducers are listed under every group of bars. In each group, the gray bar represents the population percentage of bacteria that is in the no-fluorescence state; the red bar represents the percentage in the red state, and the green bar for the green state. (b),(c) FACS dot plots in conditions B and C marked in partition (a). Regions Q1, Q3, Q4 correspond to green-, no-, red-fluorescence states, respectively. (d) The restabilized differentiation ratios after sorting. The source regions are listed under every group of bars, from which the bacteria are sorted separately.

(1 nmol/mL IPTG + 15 ng/mL aTc) [17], both green- and red-fluorescence states appear separately in a part of the bacteria with nearly the same population ratio as that of no-fluorescence state; hence, three states coexist within the same population [Fig. 3(c)]. All conditions chosen here [Fig. 3(a)] are nearly symmetric for the proportion green:red = 1:1. Results in asymmetric conditions, and systematic experimental data in a variety of conditions are shown in Supplemental Material [13] with appendixes.

One should note that 1 nmol/mL (1 μM) IPTG is an uncommonly low inducing concentration comparing with common threshold: 0.1–1 mM [3,18,19]. In those works, 1 μM IPTG had no effect; but our system is supersensitive to such a low concentration. More details of this exceptional and useful phenomenon will be presented later. The concentration of aTc used in our experiments is not order-of-magnitude different than commonly used values: 50–100 ng/mL [18,20], because 15 ng/mL aTc approximates to 0.032 μM, which is already 30-fold lower than 1 μM.

To confirm whether the differentiating behavior is robust under a certain condition of inducers, bacteria in three different states are sorted (separated) from the same population by FACS technology. Then they are recultured separately in the same condition. After restabilization, each of them differentiates into three coexisting states again, and their differentiation ratios are shown in Fig. 3(d), which have no significant change from original one before sorting. Such sorting and reculturing processes are performed in different conditions, which reveal that the additional low- or no-fluorescence state is an intrinsic and robust kinetic characteristic in our system.

The above experimental observations demonstrate that the behavior of such a small system is quite different from what a fully deterministic model could predict. Intuitively, one may expect that it is because of the internal noise (fluctuation). Usually, we can account for the internal noise by using CLEs, which are in the continuous form, or directly by using KMC discrete simulation. In our work, we have performed KMC simulations based on the processes listed in Table S1 in the Supplemental Material [13]. The two-dimensional probability distribution functions (PDFs) in the A-B plane are shown in the bottom layer of Fig. 1, consistent with the experiments. However, the CLE simulations according to Eq. (1) or the original high-dimensional ODE model (Table S2 [13]) cannot reproduce such PDFs, as shown in the top layer of Fig. 1. Hence, besides fluctuation, there must be some more features inherent in such a small system that contribute to the additional kinetic stability.

To elucidate this point, we have generated a kind of stochastic average nullclines from the KMC results. By constraining the particle number of species A to be a constant value n_A, we can get B's stationary conditional distribution $p(B|A = n_A)$, as shown by the inset

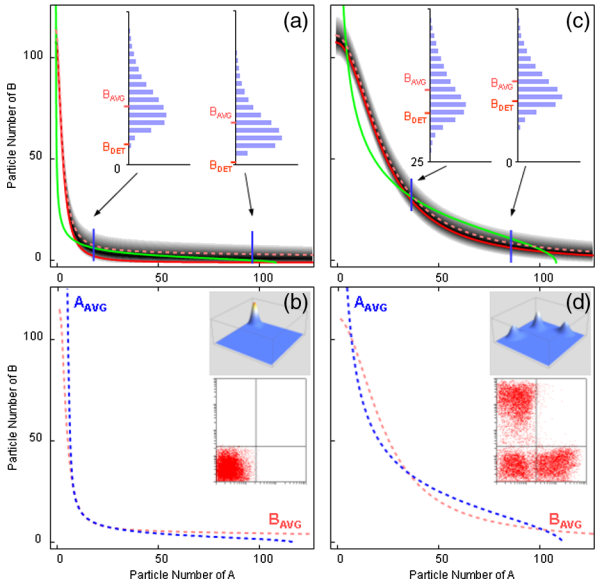

FIG. 4 (color online). Deterministic nullclines (solid curves) of species A and B, and their stochastic counterparts (dashed curves). Each stochastic one is generated by a series of mean values from stationary conditional distributions, which are shown in the inset histograms. (a),(b) without induction and (c),(d) with appropriate induction.

one-dimensional PDFs in Fig. 4(a). Here the repressing coefficient $R = 60$ corresponds to strong repressing case without inducers as in Fig. 3(b). The mean value of B's number calculated from this one-dimensional PDF—B_{AVG}, and that from the deterministic ODE—B_{DET}, are marked in every inset. By scanning the value of n_A, we can obtain a set of B_{AVG} values, which construct the stochastic average nullcline of species B, as shown by the pink dashed curve in Figs. 4(a) and 4(b). We can also obtain the stochastic average nullcline of species A, which is given by the blue dashed curve A_{AVG} in Fig. 4(b). The corresponding deterministic nullclines are drawn in Fig. 4(a) for comparison, whose three intersections related to the three steady states are also marked in Fig. 1 The gray-scale image is combined from one-dimensional PDFs with rescaling; please refer to the Supplemental Material [13] for large images and detailed procedures.

The key point one needs to realize is that the experimentally observed states should be associated with the intersections of two stochastic nullclines, rather than those of the deterministic ones. As shown obviously in Fig. 4(b), stochastic nullclines intersect at only one point near the deterministic USS point, corresponding to the no-fluorescence state. The insets of Fig. 4(b) are its relevant population distributions obtained from KMC simulation (top) and experiment (bottom).

Refer to Fig. 4(a); one can figure out why there is only one intersection. First, the conditional PDF $p(B|A = n_A)$ is clearly non-Gaussian as shown by histograms—it peaks at a low number of B and skews to the larger side; hence, it is

a positive skewed discrete distribution. Consequently, B's stochastic nullcline always positively deviates from its deterministic one; nevertheless, the relative deviation is more significant when deterministic value B_{DET} is close to zero. For instance, it (pink dashed) is much higher than B_{DET} (red solid) near the lower-right deterministic SSS point in Fig. 4(a), since the B_{DET} value asymptotic to zero cannot be experimentally reached. Similar deviation also appears on species A, and these deviations lead to the single intersection. This is caused by discrete skewed distributions of molecule numbers instead of continuous symmetric ones, when the molecules of pivotal species are very few in small chemical reaction systems [21,22].

In our system, the pivotal species' molecule numbers (such as P_a* and P_b* in Table S1) often hop between 0 and 1, occasionally 2 or more while in strong repressing condition. The fluctuation produced by hopping on the verge of extinction should naturally be described as Poisson distributed noise, but not the Gaussian one that is used in the CLE method. The positive skewness of Poisson distribution is amplified by catalytic cascade reactions in this reaction network, then finally brings on positive deviation between B_{AVG} and B_{DET}. This kind of deviation is also called ''leakage'' in expressing of a repressed promoter [23]. Positive skewed distribution of fluctuation is native in small systems when one uses discrete exact simulation methods such as KMC simulations. We emphasize here that stochastic simulations via CLE method cannot reproduce these results, unless by using non-Gaussian noise terms [24,25].

In Figs. 4(c) and 4(d), coefficient $R = 0.6$ corresponds to a weak repressing condition with a very low concentration of inducers as in Fig. 3(c). In this case, there are three intersections between two stochastic nullclines, which are related to the three experimentally observed states. One should note that the intersections of stochastic nullclines are all stable in statistical sense, as shown by the inset two-dimensional PDFs. This is because each stochastic average nullcline indicates the region around which the population peaks pronouncedly in one coordinate direction; thus, each intersection indicates a mainly distributed area in both directions. In contrast to the deterministic prediction, the middle intersection corresponds to a deterministic USS, which should not be presented; thereby, it might be called a discreteness-induced stable stochastic steady state (or attractor) [11,26].

According to the above discussions, one may conclude that it is the combined effects of the discrete, fluctuate, and non-negative features of molecular numbers in such a small system that result in the additional kinetic stability observed in our experiments.

Now we can explain the reason why our experimental system is supersensitive to such an uncommonly low inducing concentration. Briefly speaking, the inducers used here virtually play subtle roles as triggers, which change the system from the additional stable state (silent state) to either of the two unilaterally expressing states. In traditional purposes, the inducer must drive changes from a unilaterally expressing state to the opposite one. In our system, triggering from the ''silent'' state is much easier, because there are few repressor molecules expressed that need to be antagonized by inducer. The additional kinetic stable state in this toggle switch system is just like the transition state in reaction dynamics, from which the system could turn to both directions easily. Such a mesoscopic mechanism can be taken advantage of to achieve useful functions that a macroscopic system cannot achieve conveniently. For example, the function supersensitivity may be found in nature, or be used artificially for constructing biosensors. (Refer to the Supplemental Material [13] for all experimental details.)

In summary, our findings experimentally and theoretically provide a clear example that discreteness and fluctuation, particularly at low molecular concentration, might lead to additional kinetic stable states in small systems. The subtle role of discreteness and fluctuation has general importance not only in a living cell, but also in other kinds of small reaction systems that have pivotal molecules fluctuating on the verge of extinction (e.g., some microreactors, vesicles, active sites). Synthetic biological systems in living cells are a good practical platform to investigate similar effects of small systems; on the other hand, designs for synthetic biological networks should also take this issue seriously.

Furthermore, small-number effects can bring on useful functions for small systems—supersensitivity is an instance. Tristability itself may also be useful, for example, genetic tristate elements can be found or used in various biochemical networks. Stem cells and other kinds of multipotent cells might have their genes interlock in this silent state before differentiation.

We thank Prof. You Lingchong and Hong Jiong for suggestions on experiments. Thanks to KD-50-I super computer project. This work was supported by NSFC No. 21125313, No. 20933006, and No. 91027012; Chinese Ministry of Science and Technology Grant No. 2006AA02Z303 and No. 2011CBA00801.

*hzhlj@ustc.edu.cn
†hyliu@ustc.edu.cn

[1] W. Weber and M. Fussenegger, Nat. Rev. Genet. **13**, 21 (2012).
[2] W. C. Ruder, T. Lu, and J. J. Collins, Science **333**, 1248 (2011).
[3] T. S. Gardner, C. R. Cantor, and J. J. Collins, Nature (London) **403**, 339 (2000).
[4] R. Sekine, M. Yamamura, S. Ayukawa, K. Ishimatsu, S. Akama, M. Takinoue, M. Hagiya, and D. Kiga, Proc. Natl. Acad. Sci. U.S.A. **108**, 17969 (2011).

[5] B. Munsky, G. Neuert, and A. van Oudenaarden, Science **336**, 183 (2012).
[6] D. J. Wilkinson, Nat. Rev. Genet. **10**, 122 (2009).
[7] G. Balázsi, A. van Oudenaarden, and J. J. Collins, Cell **144**, 910 (2011).
[8] A. Eldar and M. B. Elowitz, Nature (London) **467**, 167 (2010).
[9] C. Tan, P. Marguet, and L. You, Nat. Chem. Biol. **5**, 842 (2009).
[10] A. Lipshtat, A. Loinger, N. Q. Balaban, and O. Biham, Phys. Rev. Lett. **96**, 188101 (2006).
[11] D. Schultz, A. M. Walczak, J. N. Onuchic, and P. G. Wolynes, Proc. Natl. Acad. Sci. U.S.A. **105**, 19165 (2008).
[12] M. Strasser, F. J. Theis, and C. Marr, Biophys. J. **102**, 19 (2012).
[13] See Supplemental Material at http://link.aps.org/supplemental/10.1103/PhysRevLett.109.248107 for more details about experiments, modeling, and simulations, including some data-set files and model files.
[14] K. Sneppen, S. Krishna, and S. Semsey, Annu. Rev. Biophys. **39**, 43 (2010).
[15] The inducers' effects are represented in the change of coefficients r_a and r_b. For example, when there are inducer molecules in concentration $\sim 9/K_I$ (K_I: association constant), effective repressing concentration $[B]$ would be reduced to $[B]/10$. Consequently, $r_a[B]^2$ becomes $r_a([B]/10)^2 = 0.01 r_a[B]^2$. It is equivalent to reduce r_a 100-fold while we keep using total concentration $[B]$ instead of effective one ($[B]/10$).
[16] Y. Rondelez, Phys. Rev. Lett. **108**, 018102 (2012).
[17] IPTG is isopropyl β-D-1-thiogalactopyranoside and aTc is anhydrotetracycline.
[18] R. Lutz and H. Bujard, Nucleic Acids Res. **25**, 1203 (1997).
[19] E. Fung, W. W. Wong, J. K. Suen, T. Bulter, S. Lee, and J. C. Liao, Nature (London) **435**, 118 (2005).
[20] S. Ehrt, X. V. Guo, C. M. Hickey, M. Ryou, M. Monteleone, L. W. Riley, and D. Schnappinger, Nucleic Acids Res. **33**, e21 (2005).
[21] Y. Togashi and K. Kaneko, Phys. Rev. Lett. **86**, 2459 (2001).
[22] J. P. Aparicio and H. G. Solari, Phys. Rev. Lett. **86**, 4183 (2001).
[23] C. M. Ghim and E. Almaas, Phys. Rev. Lett. **103**, 028101 (2009).
[24] R. Zwanzig, J. Phys. Chem. B **105**, 6472 (2001).
[25] B. M. Grafov, Russ. J. Electrochem. **39**, 999 (2003).
[26] Y. Togashi and K. Kaneko, Physica (Amsterdam) **205D**, 87 (2005).